4506–4514 *Nucleic Acids Research, 2006, Vol. 34, No. 16* *Published online 31 August 2006*
doi:10.1093/nar/gkl616

Crystallization and characterization of the thallium form of the *Oxytricha nova* G-quadruplex

Michelle L. Gill[1], Scott A. Strobel[1,2,*] and J. Patrick Loria[2,*]

[1]Department of Molecular Biophysics and Biochemistry, Yale University, New Haven, CT 06520, USA and [2]Department of Chemistry, Yale University, New Haven, CT 06520, USA

Received June 20, 2006; Revised and Accepted August 4, 2006

ABSTRACT

The crystal structure of the Tl^+ form of the G-quadruplex formed from the *Oxytricha nova* telomere sequence, $d(G_4T_4G_4)$, has been solved to 1.55 Å. This G-quadruplex contains five Tl^+ ions, three of which are interspersed between adjacent G-quartet planes and one in each of the two thymine loops. The structure displays a high degree of similarity to the K^+ crystal structure [Haider *et al.* (2002), *J. Mol. Biol.*, 320, 189–200], including the number and location of the monovalent cation binding sites. The highly isomorphic nature of the two structures, which contain such a large number of monovalent binding sites (relative to nucleic acid content), verifies the ability of Tl^+ to mimic K^+ in nucleic acids. Information from this report confirms and extends the assignment of ^{205}Tl resonances from a previous report [Gill *et al.* (2005), *J. Am. Chem. Soc.*, 127, 16 723–16 732] where ^{205}Tl NMR was used to study monovalent cation binding to this G-quadruplex. The assignment of these resonances provides evidence for the occurrence of conformational dynamics in the thymine loop region that is in slow exchange on the ^{205}Tl timescale.

INTRODUCTION

G-quadruplexes are four-stranded structures formed from DNA or RNA sequences containing tandem G-rich repeats. Sequences capable of forming G-quadruplexes *in vitro* have been identified in the telomeres of various organisms (1–9) where they are typically separated by short stretches of pyrimidines. Their location within telomeric DNA sequences has lead to the proposal that G-quadruplexes may be responsible for maintaining chromosomal integrity and chromatid pairing during mitosis (10). G-quadruplexes have also been the target of cancer research (11–14) because telomerase, the ribonucleoprotein responsible for telomere maintenance, is often found at elevated levels in cancerous cells (15,16). Other sequences shown to form G-quadruplexes *in vitro* have been identified in immunoglobulin switch regions (17) and in several gene promoters (18,19); however the biological relevance of these sequences has yet to be demonstrated conclusively.

G-quadruplexes are characterized by consecutive stacks of four planar, hydrogen-bonded guanine nucleotides, called G-quartets (Figure 1). The number of G-quartets contained within a single quadruplex varies, as does the number of distinct oligonucleotide strands that comprise the quadruplex. If less than four separate strands are involved, they fold back upon themselves leaving pyrimidine-rich unpaired loops. There is a considerable amount of heterogeneity in the location and conformation of these loops structures.

G-quadruplexes are stabilized by the binding of monovalent cations, such as Na^+, K^+, NH_4^+, Rb^+ and Tl^+ (2,5,20–32). However, the number and location of these binding sites appears to be cation specific. K^+, NH_4^+, Rb^+ and Tl^+ ions bind between adjacent G-quartet planes (23,24,27,28, 30–32). Na^+, presumably because of its smaller ionic radius, has been reported to bind both between consecutive G-quartet planes and within a single plane, although single plane binding may be preferred (2,26,28,30,33). K^+ has also been observed bound to G-quadruplex loops (23), while NH_4^+ reportedly does not bind to the loops of the same G-quadruplex (31).

We recently reported the use of ^{205}Tl NMR to directly study the binding of $^{205}Tl^+$ to the G-quadruplex formed from the *Oxytricha nova* telomere sequence, $d(G_4T_4G_4)_2$ (34), whose solution structure in the presence of Na^+ was first reported by Smith and Feigon (5). Tl^+ is a K^+ surrogate with the advantage of being a spin-1/2 nucleus with a high gyromagnetic ratio. Thus, its binding to biomacromolecules can be directly observed by solution NMR. The ^{205}Tl directly detected NMR spectrum of $d(G_4T_4G_4)_2$ contained a cluster of four downfield resonances (described as peaks 1–4, Figure 2A) that correspond to $^{205}Tl^+$ ions bound specifically by the G-quadruplex, and an intense upfield peak resulting from $^{205}Tl^+$ free in solution (data not shown) (34). Peaks

*To whom correspondence should be addressed. Tel: +1 203 436 4847; Fax: +1 203 432 6144; Email: patrick.loria@yale.edu
*Correspondence may also be addressed to Scott A. Strobel. Tel: +1 203 432 9772; Fax: +1 203 432 5767; Email: scott.strobel@yale.edu

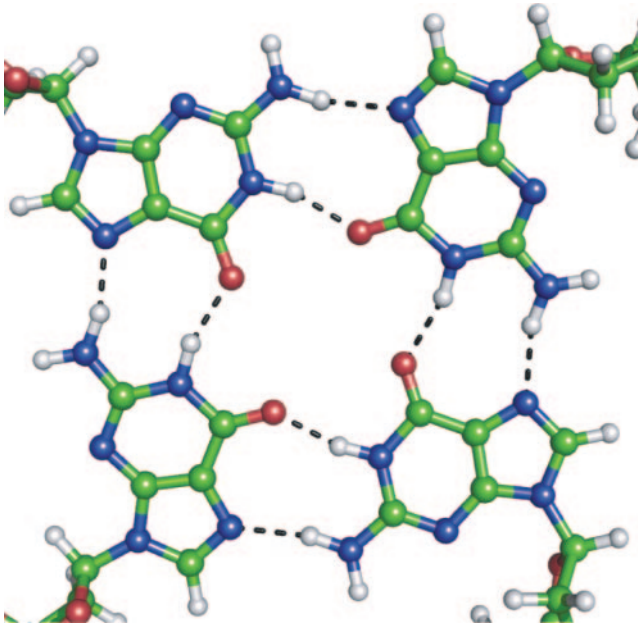

Figure 1. Schematic of a G-quartet plane formed by hydrogen bonding along the Hoogsteen and Watson–Crick faces of four guanines. Carbon atoms are shown in green, hydrogens are white, nitrogens are blue, oxygens are red and hydrogen bonds are drawn as black dashed lines.

2 and 3 were assigned to the outer and inner binding sites, respectively, (Figure 2B) within the G-quadruplex channel based on the identities of observed ^{1}H–^{205}Tl scalar couplings. Only one peak was observed for the outer binding site because a rotational symmetry operator bisects the region between the centermost two G-quartet planes of $d(G_4T_4G_4)_2$. ^{1}H–^{205}Tl scalar (J) couplings were not observed for two of the ^{205}Tl resonances, therefore their assignment in the G-quadruplex structure could not be definitively ascertained.

Based on crystallographic studies of monovalent binding to G-quadruplexes, the most likely assignment for the remaining ^{205}Tl peaks is in the thymine loops and/or along the G-quadruplex grooves. The presence of K^+ ions in the thymine loops was predicted based on NMR studies of a related G-quadruplex, $d(G_3CT_4G_3C)_2$ (35), and is consistent with a crystal structure of the K^+-form of $d(G_4T_4G_4)_2$ (23). However, solution studies of $^{15}NH_4^+$-form indicated that only three ammonium ions, all inside the G-quadruplex channel, are coordinated by $d(G_4T_4G_4)_2$ (31). There are also examples of monovalent cation binding, including Tl^+, in both the major (36,37) and minor (25,36,38–40) grooves of B-form DNA duplexes. Thus, despite their importance for G-quadruplex formation, the interaction of monovalent cations with these structures remains somewhat ambiguous.

To gain a greater understanding of monovalent cation binding to nucleic acids, to further demonstrate the ability of Tl^+ to specifically mimic K^+, and to complete the assignment of unknown ^{205}Tl resonances, we have crystallized the Tl^+-form of $d(G_4T_4G_4)_2$ and determined the location of all Tl^+ binding sites. When considered in light of this crystallographic data, we propose that the unassigned peaks in the ^{205}Tl NMR spectrum of $d(G_4T_4G_4)_2$ provide spectroscopic evidence for the occurrence of conformational dynamics within the loop region.

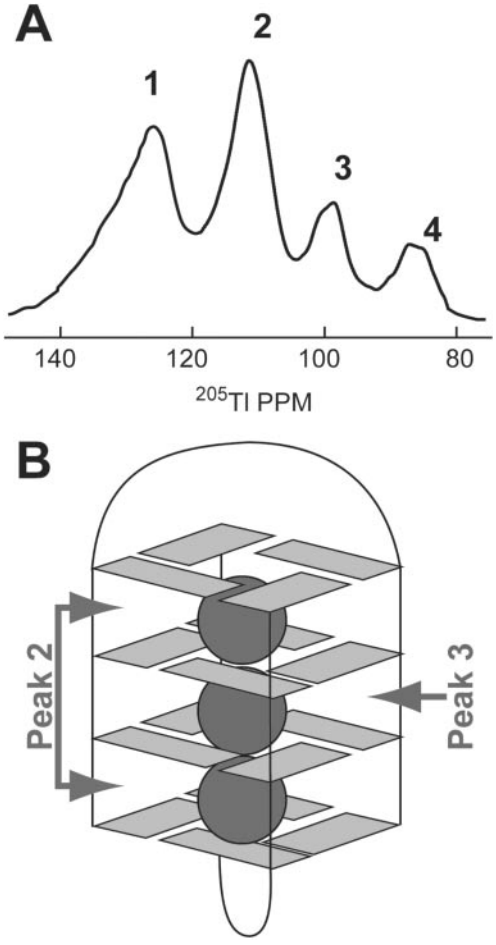

Figure 2. (**A**) Downfield region of the ^{205}Tl NMR spectrum of $d(G_4T_4G_4)_2$ showing peaks (1–4), which correspond to $^{205}Tl^+$ ions bound to the G-quadruplex (34). (**B**) The assignment of peaks 2 and 3 based on ^{1}H–^{205}Tl scalar couplings (34).

MATERIALS AND METHODS

Crystallization conditions

DNA oligonucleotides d(GGGGTTTTGGGG) were purchased (W. M. Keck Facility, Yale University) and desalted using Sep-Pak C_{18} cartridges (Waters, USA) and eluted with 40% (v/v) acetonitrile/water. After lyophilization, the DNA was dissolved to a final concentration of 10 mM in H_2O.

The crystallization conditions are listed in Table 1. The crystallization buffer, 50 mM potassium cacodylate, was made by adjusting the pH of cacodylic acid to 6.5 using potassium hydroxide and then diluting the solution to the appropriate concentration (50 mM). The final concentration of K^+ in the buffer was ~85 mM.

G-quadruplex formation was facilitated by heating d(GGGGTTTTGGGG), potassium acetate, potassium cacodylate and H_2O to 358 K for 15 min followed by slow cooling to 277 K. The DNA concentration during annealing was ~2.14 mM. After annealing, appropriate amounts of magnesium acetate, spermine and 2-methyl-2,4-pentanediol (MPD) were added to the crystallization solution, making the final DNA concentration 1.5 mM. The solution was then centrifuged at 14 000 *g* for 30 min to remove any precipitate. Crystals were grown

Table 1. Crystallization conditions for the Tl^+-form of $d(G_4T_4G_4)_2$

Crystallization components	
Potassium cacodylate pH 6.5 (mM)	50.0
Magnesium acetate (mM)	10.0
Potassium acetate (mM)	40.0
Spermine (mM)	3.5
DNA (mM)	1.5
MPD (%, v/v)	5.0
MPD (%, v/v) in well	35.0
Soaking and cryoprotection	
Thallium acetate (mM)	50.0
MPD (%, v/v)	60.0

Table 2. Crystallographic data for the Tl^+-form of $d(G_4T_4G_4)_2$

Crystallographic data	
Space group	$P2_12_12_1$
Cell dimensions a, b, c (Å)	27.375, 48.210, 96.198
α, β, γ (°)	90.000, 90.000, 90.000
Wavelength (Å)	0.979
Resolution range (Å)	43.11−1.55 (1.61−1.55)
Maximum resolution (Å)	1.44
Completeness (%)	95.0 (98.1)
Mosacity	1.252
R_{merge}	0.187(>1)
Net $I/\sigma(I)$	6.43 (22.7)
No. unique reflections	9380
R-factor (%)	22.7
R_{free} (%)	24.7
F.O.M. (%)	80.6
RMS bond distance (Å)	0.010
RMS bond angles (°)	1.901
RMS chiral (°)	0.069
No. DNA strands/asymmetric unit	4
No. Tl^+ ions	10
Average B-factor (Å^2)	
G-quartets	27.68
Loops	31.10
Tl^+ ions	32.45

using the hanging drop method (2 μl drops) at 291 K and appeared after 6–8 weeks as clear, rod-like crystals. The crystals were soaked in solutions containing 60% MPD and 50 mM thallium acetate for 2 h at 291 K prior to freezing in liquid nitrogen.

Structure determination

Data were collected on beamline X25 at the National Synchrotron Light Source at 0.9780 Å wavelength and diffraction was observed to 1.55 Å. The data were integrated and scaled using the HKL 2000 package (41). Experimental phases were determined using molecular replacement with the orthorhombic crystal structure determined by Neidle and coworkers (23) (PDB 1JRN). The space group ($P2_12_12_1$) and unit cell dimensions were similar to the published structure (Table 2). Refinement was performed using Refmac5 (42–45) in the CCP4 program suite (46). Several cycles of rigid body refinement were followed by restrained refinement using TLS parameters, resulting in an R-factor of 24.9%. One final round of restrained refinement was performed using anisotropic B-factors, further reducing the R-factor to 22.7%.

Thallium binding sites were determined after molecular replacement based on the presence of large, unoccupied peaks present in both the $2F_o - F_c$ and anomalous maps. The thallium ions were assigned to regions containing strong density in the anomalous map. Coot was used for water assignment and viewing of all density maps (47). The PDB accession code for the structure is 2HBN.

NMR CPMG-relaxation dispersion experiments

NMR experiments were performed on a 14.1 T Varian Inova instrument equipped with a triple-resonance room temperature probe and *xyz* gradients at an experimental temperature of 10°C. The temperature was calibrated with 100% methanol. Relaxation dispersion experiments (48) were performed on the methyl groups of thymine using a 2.5 mM sample of the G-quadruplex d(GGGGTTTTGGGG) containing 50 mM thallium acetate. The NMR experiment was of the constant relaxation time version (49) with the ^1H and ^{13}C carrier frequencies placed at 1.5 and 14 p.p.m., respectively during the relaxation period. CPMG delays were 0.625, 0.714, 1.0, 1.25 (× 2), 1.67 (× 2), 3.33, 2.5 (× 2), 5.0 and 10.0 ms. Peak intensities were determined in NMRDraw (50) using the script autoFit.tcl provided with the program. Dynamics parameters were obtained by fitting dispersion equations to the experimentally determined relaxation rates as described previously (51). Methyl assignments at this lower temperature were determined by monitoring the NMR chemical shifts in a two-dimensional ^{13}C HSQC in a temperature series from 25 to 10°C.

RESULTS

Structure determination and features

The crystal structure of the Tl^+-form of $d(G_4T_4G_4)_2$ was solved to 1.55 Å from a single crystal. We were able to obtain crystals of the K^+-form using conditions (Table 1) similar to those reported by Neidle and coworkers (23) except that acetate versions were substituted for all chloride-containing crystallization components to avoid the formation of insoluble thallium chloride in later steps. The concentrations of spermine (3.5 mM) and DNA oligonucleotide (1.5 mM) were slightly different from those used for crystallization of the K^+-form (4.10 and 1.0 mM, respectively). The K^+-form was then converted to the Tl^+-form by soaking the crystals in 50 mM thallium acetate. Attempts were also made at crystallizing the Tl^+-form of $d(G_4T_4G_4)_2$ directly by substituting various concentrations of thallium acetate for potassium acetate in the crystallization solution. However, no crystals were produced from these efforts.

Experimental phases were determined by molecular replacement using the crystal structure of the K^+-form (PDB 1JRN) (23). Like the orthorhombic K^+-form, the Tl^+-form was solved in the space group $P2_12_12_1$ with unit cell dimensions that differ from the K^+-form by only 0.3–3.2% in all dimensions (Table 2). Each asymmetric unit contains two G-quadruplexes that have an RMSD of 0.24 Å. The thymine loops facilitate intermolecular packing within both the asymmetric unit and crystal lattice by forming a pair of pseudo 2-fold related hydrogen bonds between the T6 O4

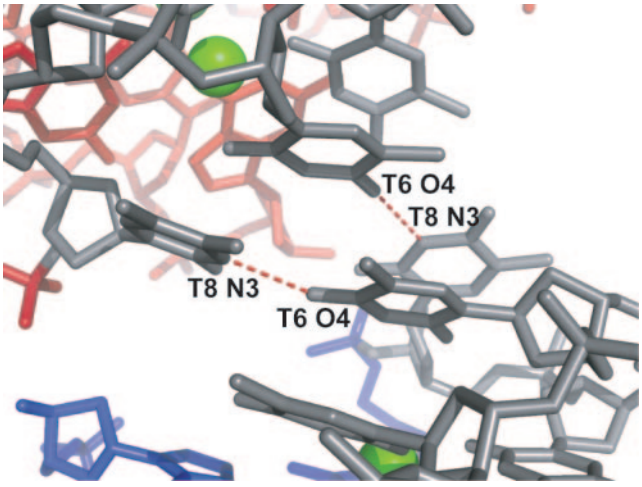

Figure 3. The asymmetric unit contains two G-quadruplexes. Crystal packing is facilitated by a pair of hydrogen bonds (red dashed lines) between T6 O4 and T8 N3. Guanosines are colored red or blue, thymines are gray and thallium ions are shown as green spheres.

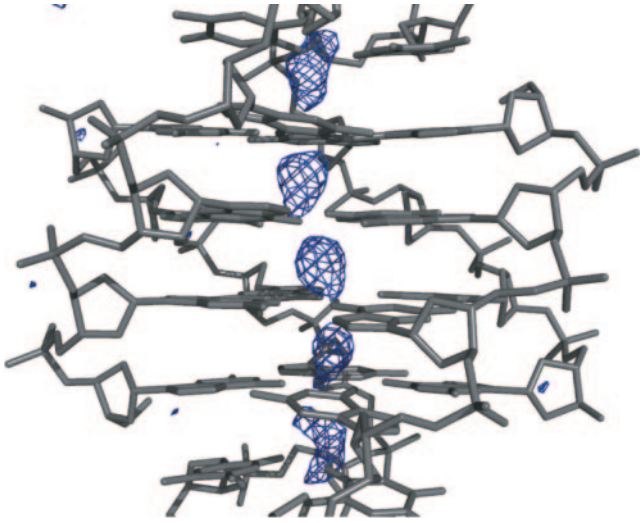

Figure 4. Anomalous density map (3.0σ) of the Tl^+ crystal structure of $d(G_4T_4G_4)_2$. The five strong peaks (blue) have been assigned to Tl^+ ions. The G-quadruplex is shown in gray.

from one G-quadruplex and the T8 N3 from the neighboring G-quadruplex (Figure 3).

The thallium ions

The assignment of metal binding sites was facilitated by the presence of strong anomalous peaks (>5.7σ) (Figure 4). Each G-quadruplex contains five bound Tl^+ ions, three interdigitated between G-quartet planes and one in each of the two loops. The average spacing between each Tl^+ ion is 3.6 Å. The relative positions of these five metals are very similar to those found in the K^+ crystal structure, where the average metal–metal spacing is reported to be 3.4 Å (23). The Tl^+ ions located between two successive G-quartet planes are coordinated by eight oxygens (one O6 from each of the surrounding guanines). These coordination distances range from 2.5–3.3 Å, which are similar to those observed in the K^+ structure (2.6–3.1 Å) (23). The Tl^+ ions bound to the loops are coordinated by four guanine O6 carbonyls from the outer G-quartet plane and two thymine carbonyls (T5 and T7 O2). The absence of any other regions of anomalous density, including the absence of density in the region surrounding the phosphate backbone, indicates that there are only five ordered Tl^+ binding sites (Figure 4).

The average B-factors for the loop-associated metals (39 $Å^2$) are higher than the other thallium binding sites (28 $Å^2$). Smaller differences in B-factors are observed in the K^+ crystal structure (23 $Å^2$ in the loops versus 20 $Å^2$ in the channel) (23). Additionally, the anomalous density in this region is less spherical (Figure 4). Accordingly, an attempt was made at refining the thallium ions located within the loops to partial occupancy. Reducing the thallium occupancy by as little as 10% produced lower B-factors and large positive peaks in the $F_o - F_c$ map. Accordingly, all thallium occupancies were left at 100%. The high degree of thallium occupancy can be explained by its ability to bind more tightly to monovalent binding sites than potassium in both proteins and nucleic acids, including G-quadruplexes (24,52–56).

The G-quartets and grooves

Each G-quartet is formed by hydrogen bonding along the Hoogsteen and Watson–Crick faces of the guanine (N2–N7 and N1–O6) with average bond lengths of 2.9 and 2.8 Å, respectively. The guanine bases have alternating *syn–anti* glycosidic bond angles and all thymines are in the *anti* conformation. The position of G4 deviates slightly from the G-quartet plane in each of the outer G-quartets. This displacement allows G4 to stack with the subsequent thymine (T5). The G-quartets in the Tl^+-form of $d(G_4T_4G_4)_2$ each contain one small, two medium and one large groove. Their average widths (C5′–C5′) are 11.1, 14.4 and 17.2 Å, which is nearly identical to the K^+ X-ray structure (23) and very similar to other diagonally looped structures (2,5,20–22,34).

The waters

A total of 44 waters were assigned to each asymmetric unit. The assignments were made in regions of unassigned density (>1.0σ) in the $2F_o - F_c$ maps that did not have any anomalous density. The number of assigned waters is considerably less than the number reported (230) for the crystal structure of the K^+-form (23). This is likely related to the use of differing criteria for the assignment of water peaks.

With respect to cation coordination, previous studies have identified that two waters participating in the coordination of the K^+ ions bound within the thymine loops in the crystal structure of $d(G_4T_4G_4)_2$ (23). Consistent with those studies, in the structure reported here one of the assigned waters in the Tl^+-form of $d(G_4T_4G_4)_2$ is located within the thymine loops and in close proximity to the loop-associated Tl^+ ion. The water–metal distance is 3.1 and 4.2 Å for the two respective G-quadruplexes located in the asymmetric unit. A second region of density within the thymine loop region was also initially assigned as water; however, this assignment could not be confirmed in our structure because the density is not resolved from the nearby Tl^+ density. Accordingly, this water assignment was deleted.

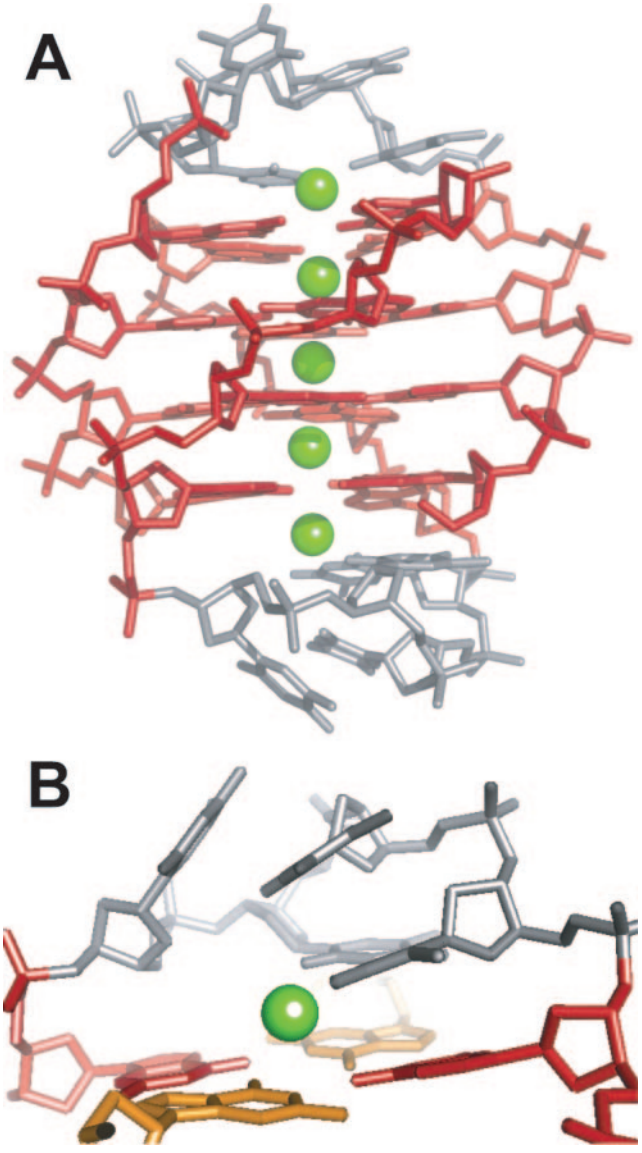

Figure 5. (**A**) Overall view of the refined crystal structure of the Tl^+-form of $d(G_4T_4G_4)_2$ (PDB ID 2HBN). Guanosines are colored red, thymines are gray and thallium ions are shown as green spheres. (**B**) Close-up of the $d(G_4T_4G_4)_2$ diagonally looped thymines. Thymines and thallium ions are as in (A). Guanosines are shown in red or orange, depending on which DNA strand they belong.

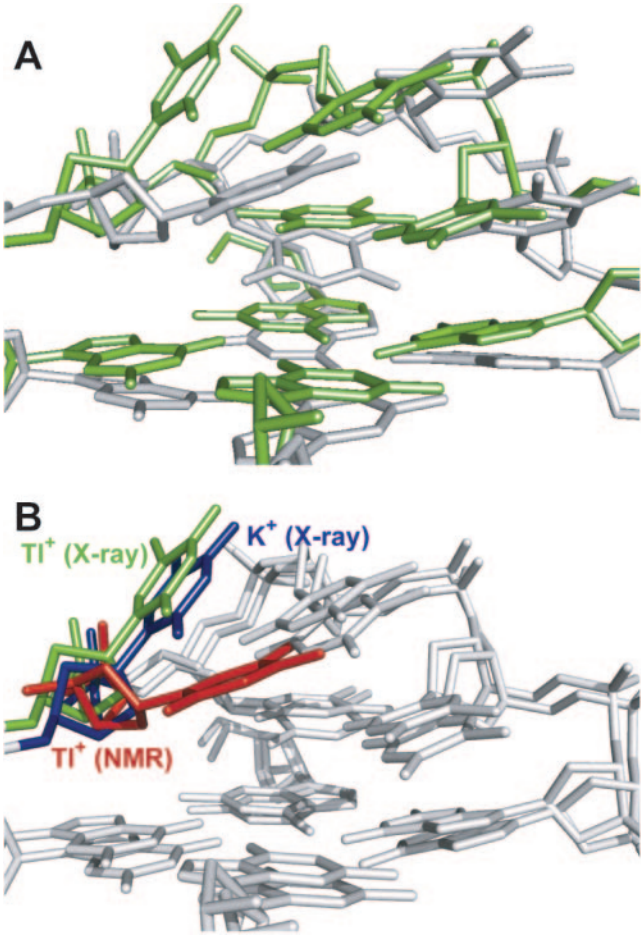

Figure 6. (**A**) The greatest variability between the Tl^+ crystal (green) and solution (PDB 2AKG, gray) structures is in the thymine loops. (**B**) Comparison of T8 in the Tl^+ crystal structure with the K^+ X-ray structure (PDB 1JRN) and the Tl^+ solution structure (PDB 2AKG). T8 is shown in green for the Tl^+ crystal structure, blue for the K^+ crystal structure and red for the Tl^+ solution structure. Other thymines and the nearby G-quartet are colored gray. For simplicity, only T8 is shown from the solution structure.

Comparison to other structures

The G-quadruplex is a homodimer containing diagonal thymine loops at both ends (Figure 5A and B). This architecture is identical to that observed in the solution structures (Na^+, K^+, Tl^+ and NH_4^+) of $d(G_4T_4G_4)_2$ (5,20–22,34), in the crystal structure of the Na^+-form in the *O.nova* protein complex (2), and in the orthorhombic and trigonal crystal structures of the K^+-form reported by Neidle and coworkers (23). The average RMSD of the Tl^+ and K^+ crystal forms is 0.26 Å. The high degree of similarity between these two crystal structures is a likely explanation for the limited effect that soaks in high concentrations of thallium (≤50 mM) have on the structural resolution.

The RMSD of the Tl crystal structure to the solution structure of the Tl^+-form of $d(G_4T_4G_4)_2$ (PDB 2AKG) is 2.16 Å (34); however, the G-quartets have an RMSD of only 1.25 Å. This suggests that the loop region is the source of the greatest amount of variability between the X-ray and solution structures (Figure 6A). In the crystal structure of the Tl^+-form, T8 is extended into solution, similar to the crystal structures of the K^+- (Figure 6B) and Na^+-forms (2,23). This is in contrast to the Tl^+ (and K^+) solution structures where T8 stacks above the neighboring G-quartet plane. This conformation in solution is supported by unambiguous NOEs between T8 and the G-quartet plane (G1, G4 and G12) (34). The effects of crystal packing could explain the differences observed in solution and crystal forms (Figures 3 and 6A). However, the presence of telomere binding protein precludes packing between G-quadruplexes in the crystal structure of the Na^+-form (2), indicating that monovalent metal identity may also play a role in defining the loop conformation.

NMR dynamics

The relative ^1H and ^{13}C peak positions of the thymine methyl do not change between 25 and 10°C and therefore their assignment is straightforward at 10°C (Figure 7A). The

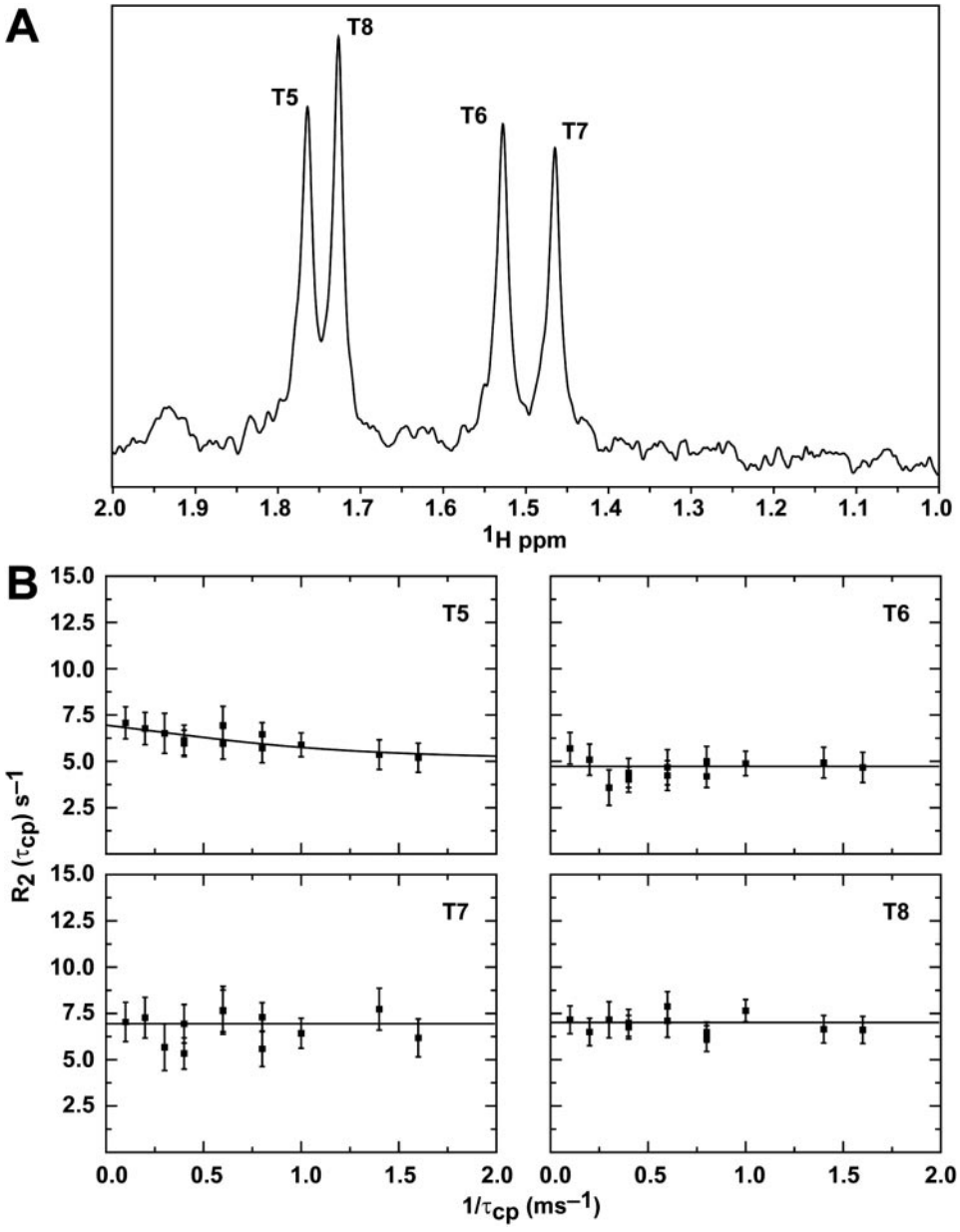

Figure 7. Thymine methyl NMR experiments. (**A**) ^{1}H aliphatic region showing the four resonances corresponding to methyl groups of the thymine loop residues. (**B**) ^{13}C-CPMG-relaxation dispersion data for each methyl carbon of the thymine loops. Only the T5 methyl group shows dispersion with τ_{cp}.

NMR relaxation dispersion experiments show evidence of conformational exchange at the methyl position of T5 in the $d(G_4T_4G_4)_2$ structure (Figure 7B). At 10°C, the conformational exchange rate, $k_{ex} = 2900 \pm 410\ s^{-1}$ and $R_{ex} = p_a p_b \Delta\omega^2 = 2.0 \pm 0.4\ s^{-1}$. At this static magnetic field strength, there is no evidence of dynamics at the other methyl positions in the thymine loops (Figure 7B).

DISCUSSION

Tl^+ binding sites in $d(G_4T_4G_4)_2$

The crystal structure of the Tl^+-form of $d(G_4T_4G_4)_2$ is very similar to the K^+ crystal structure (23), even in variable regions, such as the thymine loops, and the monovalent cation binding sites. These structural similarities and the ability of such a large number of thallium ions to replace potassium ions without disrupting the crystal lattice further verifies the isomorphous nature of Tl^+ and K^+ in nucleic acids (34,57–60) and suggests its usage as a heavy metal derivative in crystallographic studies and as a monovalent ion probe (24,25,34) is valid and non-perturbing.

The Tl^+-form of $d(G_4T_4G_4)_2$ is capable of binding three Tl^+ ions within the G-quadruplex channel and two in the thymine loops. The observation of Tl^+ ions associated in the thymine loops is in agreement with the K^+ crystal structure (23) but not with solution studies of $^{15}NH_4^+$ binding to $d(G_4T_4G_4)_2$ (20,31). Possible explanations that reconcile these data are that the thymine loops of $d(G_4T_4G_4)_2$ do not adopt a conformation in solution that can accommodate the binding

of any monovalent cations or that ammonium binds to $d(G_4T_4G_4)_2$ in a manner that is somewhat different from K^+ and Tl^+.

Thymine loop conformation

Because the loops mediate crystal packing and are the only region that differs (albeit only slightly) from the solution and crystal structures of both K^+- and Tl^+-forms, it is possible that the crystal conformation does not exist in solution and that the metal bound by the thymine loops is a crystallographic artifact. However, the involvement of this conformation in crystal packing does not rule out its existence in solution. The thymine loops have increased transverse relaxation rates (34), indicating the presence of conformational exchange in this region. Further evidence of their dynamic nature is provided by the slightly elevated B-factors observed in the loops relative to the G-quartets (Table 2). Accordingly, it is reasonable to conclude that the loop conformation observed in the crystal structure is one of several that exist in solution.

Assignment of ^{205}Tl NMR resonances

These combined crystallographic and NMR dynamics experiments can be used to gain insight into the G-quadruplex structure and to refine the assignment of ^{205}Tl resonances from the recent NMR solution study of $^{205}Tl^+$ binding to $d(G_4T_4G_4)_2$ (34). Based on these experiments, ^{205}Tl peak 1 (Figure 2) is likely binding in the thymine loops, given that ordered Tl^+ binding sites exist in the loop regions of the crystal structure. The high degree of occupancy in these binding sites is consistent with the approximate area of peak 1 relative to peaks 2 and 3.

The assignment of ^{205}Tl peak 4, which is of lower intensity, is less straightforward. No anomalous density was observed along the G-quadruplex grooves, making it unlikely that this is the explanation for the resonance corresponding to peak 4. The monovalent binding sites located within the G-quadruplex channel correspond to peaks 2 and 3 (34). Further, each of these sites displayed ^{1}H–^{205}Tl scalar couplings, which were not observed for peak 4. Thus, it is not likely that peak 4 results from $^{205}Tl^+$ binding to the G-quadruplex channel. One remaining possibility is that peaks 1 and 4 correspond to a single Tl^+ ion bound to a conformationally mobile thymine loop resulting in two, distinct ^{205}Tl resonances separated by 40 p.p.m., which is reasonable considering the extremely large ^{205}Tl chemical shift range (~7000 p.p.m.) (61). This assignment to the thymine loop is in agreement with the aforementioned data indicating that these loops are in conformational exchange and could also be the reason that ^{1}H–^{205}Tl scalar couplings were not observed for peaks 1 and 4.

However, the assignment of two ^{205}Tl peaks to the loop binding sites initially seems inconsistent with the symmetry of this G-quadruplex (25,31,34). Because of this 2-fold symmetry, only one ^{1}H resonance is observed for each proton in the G-quartet and in the loop (5,20–22,34). In addition, only a single ^{205}Tl resonance is observed for the $^{205}Tl^+$ ions bound to the two outer G-quadruplex binding sites (34). Thus, the Tl^+ binding sites located in the thymine loops would be expected to be magnetically equivalent as well, resulting in only one ^{205}Tl peak for the loop-associated binding sites.

This apparent discrepancy can be explained by taking note of the more generous limit on slow conformational exchange imposed by the large ^{205}Tl chemical shift range. The appearance of a resonance in an NMR spectrum for a nucleus in a conformational exchange process depends on the relation between the rate of exchange (k_{ex}) and the chemical shift difference ($\Delta\omega$) for the assumed, two exchanging conformations (62). If the exchange rate is less than $\Delta\omega$ (slow exchange) two resonances are observed at the chemical shift values of the individual conformations. If, on the other hand, $k_{ex} > \Delta\omega$ (fast exchange) a single resonance is observed at a population weighted chemical shift. We propose that peaks 1 and 4 (Figure 2A) are in the slow exchange regime (two peaks) on the thallium chemical shift timescale whereas the ^{1}H resonances in these conformational mobile loops are in the fast exchange regime (one peak), thereby resolving the noted discrepancy. This allows estimation of the time scale for conformational motion of these loops. At 25°C, the separation between the two downfield ^{205}Tl resonances (peaks 1 and 4) is ~40 p.p.m., $\Delta\omega \approx 72\,000\ s^{-1}$ at 11.7 T, thereby placing an upper limit on the exchange rate for a slowly exchanging thallium ion. Even if a generous chemical shift difference of 2 p.p.m. is considered for an exchanging proton, $\Delta\omega \approx 6000\ s^{-1}$ at 11.7 T, which is 1/12 of the limit on the ^{205}Tl timescale. This places a lower limit on the exchange rate on the ^{1}H time scale. Thus, it is possible that a conformationally exchanging thymine loop could be moving on a timescale that would give rise to slow exchange on the ^{205}Tl timescale and fast exchange on the ^{1}H timescale if the exchange rate was between 10^3–$10^4\ s^{-1}$. In order to observe two separate ^{1}H resonances in an exchange process on this time scale they would have to be separated by over 22 p.p.m., which is larger than the diamagnetic ^{1}H chemical shift range.

To obtain experimental evidence concerning the thymine loop dynamics, NMR relaxation dispersion experiments were performed (63). Because the thallium signal-to-noise is insufficient to accurately measure conformational exchange on this timescale, we attempted to characterize the loop dynamics by using CPMG-dispersion experiments at the methyl positions in the thymine loop residues. If these loops are dynamic the methyl position should be sensitive to its motion. The data in Figure 7B clearly show increasing (dispersion) $R_2(1/\tau_{cp})$ values for T5 as the spin-echo delay increases. The resulting dynamics parameters indicate an exchange rate for T5 of $2900\ s^{-1}$ at 10°C. If the exchange rate at 25°C is estimated by the so-called '$Q_{10} = 2$' rule (64) k_{ex} would be $\sim 10\,000\ s^{-1}$, a rate in line with the argument of a motional process in slow exchange with respect to thallium but fast on the proton chemical shift time scale. It should be noted that the exact exchange rate at 25°C (the temperature at which ^{205}Tl NMR experiments were performed) is not known. For technical reasons the CPMG-dispersion experiment cannot determine exchange rates $\geqslant 10^4$ therefore they were performed at a lower temperature where the exchange rate was estimated to be in the measurable range based on our calculations and observations at 25°C. This conclusion suggests that the areas of peaks 1+4 should equal peak 2 (and 2 × peak 3). Quantitation of peak areas is difficult

due to the large linewidths, baseline distortions from the large free Tl resonance, disordered Tl^+ binding along the quadruplex grooves, and the non-Lorentzian shape of peak 4. Nevertheless considering all these factors, qualitative estimates provide peak areas consistent with the exchange scenario described above. In summary the dispersion experiments are completely consistent with a flexible thymine loop resulting in a thallium nucleus experiencing two distinct magnetic environments on a time scale that allows observation of separate ^{205}Tl resonances.

We have crystallized the Tl^+-form of $d(G_4T_4G_4)_2$ and demonstrated that it binds five Tl^+ ions in a manner that is nearly identical to the previously reported K^+ crystal structure (23). These results demonstrate that $^{205}Tl^+$ ions bind within the G-quadruplex thymine loops in a manner similar to K^+ and are observable by direct detection ^{205}Tl NMR (34). The combination of knowledge from X-ray crystallography and solution NMR of all existing Tl^+ binding sites has led to the proposal that multiple loop conformations exist, at least two of which bind Tl^+. The complementary nature of these two spectroscopic techniques provides additional insight on monovalent cation binding to the conformationally flexible G-quadruplex.

ACKNOWLEDGEMENTS

The authors thank M. Becker and the staff at Brookhaven National Laboratory Beamline X25 for help with data collection and the staff at the Yale University Center for Structural Biology, especially Dr Michael Strickler, for help with refinement. Jesse Cochrane, Mary Stahley and Sarah Lipchock provided helpful scientific discussion. This research was supported by NIH R01 GM61239 to S.A.S. and J.P.L. M.L.G. acknowledges support from an NSF graduate fellowship. Funding to pay the Open Access publication charges for this article was provided by NIH R01 GM61239.

Conflict of interest statement. None declared.

REFERENCES

1. Henderson,E.R. and Blackburn,E.H. (1989) An overhanging 3′ terminus is a conserved feature of telomeres. *Mol. Cell. Biol.*, **9**, 345–348.
2. Horvath,M.P. and Schultz,S.C. (2001) DNA G-quartets in a 1.86 A resolution structure of an *Oxytricha nova* telomeric protein–DNA complex. *J. Mol. Biol.*, **310**, 367–377.
3. Kang,C., Zhang,X., Ratliff,R., Moyzis,R. and Rich,A. (1992) Crystal structure of four-stranded *Oxytricha* telomeric DNA. *Nature*, **356**, 126–131.
4. Oka,Y. and Thomas,C.A., Jr (1987) The cohering telomeres of *Oxytricha*. *Nucleic Acids Res.*, **15**, 8877–8898.
5. Smith,F.W. and Feigon,J. (1992) Quadruplex structure of *Oxytricha* telomeric DNA oligonucleotides. *Nature*, **356**, 164–168.
6. Williamson,J.R., Raghuraman,M.K. and Cech,T.R. (1989) Monovalent cation-induced structure of telomeric DNA: the G-quartet model. *Cell*, **59**, 871–880.
7. Williamson,J.R. (1994) G-quartet structures in telomeric DNA. *Annu. Rev. Biophys. Biomol. Struct.*, **23**, 703–730.
8. Parkinson,G.N., Lee,M.P. and Neidle,S. (2002) Crystal structure of parallel quadruplexes from human telomeric DNA. *Nature*, **417**, 876–880.
9. Wang,Y. and Patel,D.J. (1993) Solution structure of the human telomeric repeat $d[AG_3(T_2AG_3)_3]$ G-tetraplex. *Structure*, **1**, 263–282.
10. Neidle,S. and Parkinson,G.N. (2003) The structure of telomeric DNA. *Curr. Opin. Struct. Biol.*, **13**, 275–283.
11. Han,H. and Hurley,L.H. (2000) G-quadruplex DNA: a potential target for anti-cancer drug design. *Trends Pharmacol. Sci.*, **21**, 136–142.
12. Gowan,S.M., Harrison,J.R., Patterson,L., Valenti,M., Read,M.A., Neidle,S. and Kelland,L.R. (2002) A G-quadruplex-interactive potent small-molecule inhibitor of telomerase exhibiting *in vitro* and *in vivo* antitumor activity. *Mol. Pharmacol.*, **61**, 1154–1162.
13. Read,M., Harrison,R.J., Romagnoli,B., Tanious,F.A., Gowan,S.H., Reszka,A.P., Wilson,W.D., Kelland,L.R. and Neidle,S. (2001) Structure-based design of selective and potent G quadruplex-mediated telomerase inhibitors. *Proc. Natl Acad. Sci. USA*, **98**, 4844–4849.
14. Izbicka,E., Wheelhouse,R.T., Raymond,E., Davidson,K.K., Lawrence,R.A., Sun,D., Windle,B.E., Hurley,L.H. and Von Hoff,D.D. (1999) Effects of cationic porphyrins as G-quadruplex interactive agents in human tumor cells. *Cancer Res.*, **59**, 639–644.
15. Kim,N.W., Piatyszek,M.A., Prowse,K.R., Harley,C.B., West,M.D., Ho,P.L., Coviello,G.M., Wright,W.E., Weinrich,S.L. and Shay,J.W. (1994) Specific association of human telomerase activity with immortal cells and cancer. *Science*, **266**, 2011–2015.
16. Cech,T.R. (2004) Beginning to understand the end of the chromosome. *Cell*, **116**, 273–279.
17. Sen,D. and Gilbert,W. (1988) Formation of parallel 4-stranded complexes by guanine-rich motifs in DNA and its implications for meiosis. *Nature*, **334**, 364–366.
18. Evans,T., Schon,E., Gora-Maslak,G., Patterson,J. and Efstratiadis,A. (1984) S1-hypersensitive sites in eukaryotic promoter regions. *Nucleic Acids Res.*, **12**, 8043–8058.
19. Kilpatrick,M.W., Torri,A., Kang,D.S., Engler,J.A. and Wells,R.D. (1986) Unusual DNA structures in the adenovirus genome. *J. Biol. Chem.*, **261**, 11350–11354.
20. Schultze,P., Hud,N.V., Smith,F.W. and Feigon,J. (1999) The effect of sodium, potassium and ammonium ions on the conformation of the dimeric quadruplex formed by the *Oxytricha nova* telomere repeat oligonucleotide d(G(4)T(4)G(4)). *Nucleic Acids Res.*, **27**, 3018–3028.
21. Schultze,P., Smith,F.W. and Feigon,J. (1994) Refined solution structure of the dimeric quadruplex formed from the *Oxytricha* telomeric oligonucleotide d(GGGGTTTTGGGG). *Structure*, **2**, 221–233.
22. Smith,F.W. and Feigon,J. (1993) Strand orientation in the DNA quadruplex formed from the *Oxytricha* telomere repeat oligonucleotide $d(G_4T_4G_4)$ in solution. *Biochemistry*, **32**, 8682–8692.
23. Haider,S., Parkinson,G.N. and Neidle,S. (2002) Crystal structure of the potassium form of an *Oxytricha nova* G-quadruplex. *J. Mol. Biol.*, **320**, 189–200.
24. Basu,S., Szewczak,A.A., Cocco,M. and Strobel,S.A. (2000) Direct detection of monovalent metal ion binding to a DNA G-quartet by ^{205}Tl NMR. *J. Am. Chem. Soc.*, **122**, 3240–3241.
25. Feigon,J., Butcher,S.E., Finger,L.D. and Hud,N.V. (2001) Solution nuclear magnetic resonance probing of cation binding sites on nucleic acids. *Meth. Enzymol.*, **338**, 400–420.
26. Laughlan,G., Murchie,A.I., Norman,D.G., Moore,M.H., Moody,P.C., Lilley,D.M. and Luisi,B. (1994) The high-resolution crystal structure of a parallel-stranded guanine tetraplex. *Science*, **265**, 520–524.
27. Wong,A., Ida,R. and Wu,G. (2005) Direct NMR detection of the 'invisible' alkali metal cations tightly bound to G-quadruplex structures. *Biochem. Biophy. Res. Comm.*, **337**, 363–366.
28. Wong,A. and Wu,G. (2003) Selective binding of monovalent cations to the stacking G-quartet structure formed by guanosine 5′-monophosphate: a solid-state NMR study. *J. Am. Chem. Soc.*, **125**, 13895–13905.
29. Wu,G., Wong,A., Gan,Z. and Davis,J.T. (2003) Direct detection of potassium cations bound to G-quadruplex structures by solid-state ^{39}K NMR at 19.6 T. *J. Am. Chem. Soc.*, **125**, 7182–7183.
30. Caceres,C., Wright,G., Gouyette,C., Parkinson,G. and Subirana,J.A. (2004) A thymine tetrad in d(TGGGGT) quadruplexes stabilized with Tl^+/Na^+ ions. *Nucleic Acids Res.*, **32**, 1097–1102.
31. Hud,N.V., Schultze,P., Sklenar,V. and Feigon,J. (1999) Binding sites and dynamics of ammonium ions in a telomere repeat DNA quadruplex. *J. Mol. Biol.*, **285**, 233–243.
32. Detellier,C. and Laszlo,P. (1980) Role of alkali-metal and ammonium cations in the self-assembly of the 5′-guanosine monophosphate dianion. *J. Am. Chem. Soc.*, **102**, 1135–1141.

33. Rovnyak,D., Baldus,M., Wu,G., Hud,N.V., Feigon,J. and Griffin,R.G. (2000) Localization of Na-23(+) in a DNA quadruplex by high-field solid-state NMR. *J. Am. Chem. Soc.*, **122**, 11423–11429.
34. Gill,M.L., Strobel,S.A. and Loria,J.P. (2005) ^{205}Tl NMR methods for the characterization of monovalent cation binding to nucleic acids. *J. Am. Chem. Soc.*, **127**, 16723–16732.
35. Bouaziz,S., Kettani,A. and Patel,D.J. (1998) A K cation-induced conformational switch within a loop spanning segment of a DNA quadruplex containing G-G-G-C repeats. *J. Mol. Biol.*, **282**, 637–652.
36. Howerton,S.B., Sines,C.C., VanDerveer,D. and Williams,L.D. (2001) Locating monovalent cations in the grooves of B-DNA. *Biochemistry*, **40**, 10023–10031.
37. Moulaei,T., Maehigashi,T., Lountos,G.T., Komeda,S., Watkins,D., Stone,M.P., Marky,L.A., Li,J.S., Gold,B. and Williams,L.D. (2005) Structure of B-DNA with cations tethered in the major groove. *Biochemistry*, **44**, 7458–7468.
38. Cesare Marincola,F., Denisov,V.P. and Halle,B. (2004) Competitive Na(+) and Rb(+) binding in the minor groove of DNA. *J. Am. Chem. Soc.*, **126**, 6739–6750.
39. Hud,N.V., Sklenar,V. and Feigon,J. (1999) Localization of ammonium ions in the minor groove of DNA duplexes in solution and the origin of DNA A-tract bending. *J. Mol. Biol.*, **286**, 651–660.
40. Hud,N.V., Schultze,P. and Feigon,J. (1998) Ammonium ion as an NMR probe for monovalent cation coordination sites of DNA quadruplexes. *J. Am. Chem. Soc.*, **120**, 6403–6404.
41. Otwinowski,Z. and Minor,W. (1997) Processing of X-ray diffraction data collected in oscillation mode. *Methods in Enzymology*. Academic Press, Vol. **276**, pp. 307–326.
42. Murshudov,G.N., Vagin,A.A. and Dodson,E.J. (1997) Refinement of macromolecular structures by the maximum-likelihood method. *Acta. Crystallogr. D. Biol. Crystallogr.*, **53**, 240–255.
43. Murshudov,G.N., Vagin,A.A., Lebedev,A., Wilson,K.S. and Dodson,E.J. (1999) Efficient anisotropic refinement of macromolecular structures using FFT. *Acta. Crystallogr. D. Biol. Crystallogr.*, **55**, 247–255.
44. Pannu,N.S., Murshudov,G.N., Dodson,E.J. and Read,R.J. (1998) Incorporation of prior phase information strengthens maximum-likelihood structure refinement. *Acta. Crystallogr. D. Biol. Crystallogr.*, **54**, 1285–1294.
45. Winn,M.D., Isupov,M.N. and Murshudov,G.N. (2001) Use of TLS parameters to model anisotropic displacements in macromolecular refinement. *Acta. Crystallogr. D. Biol. Crystallogr.*, **57**, 122–133.
46. Collaborative Computational Project, Number 4 (1994) The CCP4 suite: programs for protein crystallography. *Acta. Crystallogr. D. Biol. Crystallogr.*, **50**, 760–763.
47. Emsley,P. and Cowtan,K. (2004) Coot: model-building tools for molecular graphics. *Acta. Crystallogr. D. Biol. Crystallogr.*, **60**, 2126–2132.
48. Loria,J.P., Rance,M. and Palmer,A.G., III (1999) A relaxation-compensated Carr-Purcell-Meiboom-Gill sequence for characterizing chemical exchange by NMR spectroscopy. *J. Am. Chem. Soc.*, **121**, 2331–2332.
49. Mulder,F.A., Hon,B., Mittermaier,A., Dahlquist,F.W. and Kay,L.E. (2002) Slow internal dynamics in proteins: application of NMR relaxation dispersion spectroscopy to methyl groups in a cavity mutant of T4 lysozyme. *J. Am. Chem. Soc.*, **124**, 1443–1451.
50. Delaglio,F., Grzesiak,S., Vuister,G., Zhu,G., Pfeifer,J. and Bax,A. (1995) NMRPipe: a multidimensional spectral processing system based on UNIX pipes. *J. Biomol. NMR*, **6**, 277–293.
51. Beach,H., Cole,R., Gill,M. and Loria,J.P. (2005) Conservation of μs - ms enzyme motions in the apo- and substrate-mimicked state. *J. Am. Chem. Soc.*, **127**, 9167–9176.
52. Hultin,T. and Naslund,P.H. (1974) Effects of thallium (I) on the structure and functions of mammalian ribosomes. *Chem. Biol. Interact.*, **8**, 315–328.
53. Hultin,T. and Naslund,P.H. (1974) Ion binding and ribosomal conformation and function. Experiments with the K^+ analogue, Tl^+. *Acta. Biol. Med. Ger.*, **33**, 753–760.
54. Hinton,J.F., Whaley,W.L., Shungu,D., Koeppe,R.E.,2nd and Millett,F.S. (1986) Equilibrium binding constants for the group I metal cations with gramicidin-A determined by competition studies and Tl^+-205 nuclear magnetic resonance spectroscopy. *Biophys. J.*, **50**, 539–544.
55. Urry,D.W., Trapane,T.L., Venkatachalam,C.M. and Prasad,K.U. (1985) C-13 nuclear magnetic-resonance study of potassium and thallium ion binding to the gramicidin-a transmembrane channel. *Can. J. Chem.*, **63**, 1976–1981.
56. Grisham,C.M., Gupta,R.K., Barnett,R.E. and Mildvan,A.S. (1974) Thallium-205 nuclear relaxation and kinetic studies of sodium and potassium ion-activated adenosine triphosphatase. *J. Biol. Chem.*, **249**, 6738–6744.
57. Basu,S., Rambo,R.P., Strauss-Soukup,J., Cate,J.H., Ferre-D'Amare,A.R., Strobel,S.A. and Doudna,J.A. (1998) A specific monovalent metal ion integral to the AA platform of the RNA tetraloop receptor. *Nature Struct. Biol.*, **5**, 986–992.
58. Conn,G.L., Gittis,A.G., Lattman,E.E., Misra,V.K. and Draper,D.E. (2002) A compact RNA tertiary structure contains a buried backbone-K^+ complex. *J. Mol. Biol.*, **318**, 963–973.
59. Adams,P.L., Stahley,M.R., Kosek,A.B., Wang,J. and Strobel,S.A. (2004) Crystal structure of a self-splicing group I intron with both exons. *Nature*, **430**, 45–50.
60. Stahley,M.R. and Strobel,S.A. (2005) Structural evidence for a two-metal-ion mechanism of group I intron splicing. *Science*, **309**, 1587–1590.
61. Hinton,J.F. (1987) Thallium-NMR spectroscopy. *Mag. Res. Chem.*, **25**, 659–669.
62. Palmer,A.G.,3rd, , Kroenke,C.D. and Loria,J.P. (2001) Nuclear magnetic resonance methods for quantifying microsecond-to-millisecond motions in biological macromolecules. *Meth. Enzymol.*, **339**, 204–238.
63. Gutowsky,H.S., Vold,R.L. and Wells,E.J. (1965) Theory of chemical exchange effects in magnetic resonance. *J. Chem. Phys.*, **43**, 4107–4125.
64. Harcourt,A.V. (1867) On the observation of the course of chemical change. *J. Chem. Soc.*, **20**, 460–495.